SLAC-PUB-432
June 1968
(ACC)

Corrected Copy
Changed Oct. 1968

THE EFFECT OF TARGET SCATTERING ON THE SHIELDING OF HIGH ENERGY ELECTRON BEAMS*

by

T. M. Jenkins and W. R. Nelson
Stanford Linear Accelerator Center
Stanford University, Stanford, California

(Submitted to Health Physics)

*Work supported by U. S. Atomic Energy Commission

I. INTRODUCTION

In order to properly shield against high energy ($E_0 \geq 100$ MeV) accelerator radiation, a knowledge of where the electromagnetic shower, and hence the production of secondary radiation occurs, is necessary. If the beam is absorbed in a beam dump, the source is well located; however, if a thin target ($t \lesssim 0.1$ radiation lengths) is inserted into a beam, the multiple scattering of the primary particles may cause a significant fraction of the total beam power or energy to attenuate in material that is located outside a normally adequate shield.

An example of such a condition exists at SLAC where a beam dump, which is shielded for beam powers in excess of 1 MW, is located 460 feet from a thin target location. The area between the target and the beam dump is shielded for a normal electron beam power absorption of 100 W. Therefore, if 1 MW of electron beam power were sent to the beam dump, the allowable fraction that could scatter out and strike the beam transport pipe, or some similar obstacle shielded for 100 watts, would be 10^{-4}. For a greater fraction to be deposited, extra shielding would be required, provided that the area of deposition, and the fraction absorbed, were known.

This problem is common to those machines where the drift length is sufficiently long to allow a large fraction of the beam to escape, and to high intensity accelerators where even a small fraction can constitute a major radiation hazard. The SLAC 20-GeV electron accelerator is an example of both cases.

II. SCATTERING CALCULATIONS

A. Fermi-Eyges Scattering

One method of calculating the fraction of electrons that escape a given solid angle is to assume that the scattering is strictly Gaussian. From the which leads to

$$g(t\ ) = e^{-\epsilon^2/4A_o} \tag{5}$$

This is plotted as the dashed line in Fig, 1 for the case of a 0.07 r.l. copper target and an incident electron energy of 1 GeV. No single (or plural) scattering has been included.

B. Molière-NSW Scattering

A more accurate description of multiple scattering was given by Molière,[4] and improved by Nigam, et al.[5] (NSW). A simplification of the NSW theory was recently published by Marion and Zimmerman.[6] The latter give the differential distribution function as

$$F(X) = \frac{1}{X_c^2 B}\left(F_o + \frac{1}{B}F_1 + \frac{1}{2B^2}F_2\right) \tag{6}$$

where

$$F_o = 2e^{-X^2} \tag{7}$$

$$F_1 = \frac{1}{4}\int_o^{\Gamma} u^3 J_o(uX)\,\ell n\left(\frac{u^2}{4}\right)e^{-u^2/4}\,du \tag{8}$$

$$F_2 = \frac{1}{16}\int_o^{\Gamma} u^5 J_o(uX)\left[\ell n\left(\frac{u^4}{4}\right)\right]^2 e^{-u^2/4}\,du \tag{9}$$

$$\Gamma \approx \sqrt{B}\ e^{(B-1.5)/2.2} \tag{10}$$

$$B - \ell n B = b \tag{11}$$

$$b = \ell n\left[\frac{2730\,(Z+1)Z^{1/3}t}{A\beta^2}\right] - 0.1544 \tag{12}$$

The essential variable of the theory is the reduced angle, X, defined by

$$X = \theta/X_c\sqrt{B} \tag{13}$$

where
$$X_c^2 = 0.1569\left[\frac{Z(Z+1)t}{A(p\beta c)^2}\right] \tag{14}$$

A = atomic weight

Z = atomic number

p = momentum, MeV/c

For relativistic particles, the parameter B depends mainly on the foil thickness, t, in g-cm^{-2}.

Marion and Zimmerman have solved the above integrals numerically and have published a set of tables representing a family of "universal" angular distribution curves, F(X), which depend on the single parameter B. In order to calculate $g(t,\theta)$ from Eq. (3), $P(\theta)d\theta$ must be determined from the differential distribution F(X) using

$$P(\theta)d\theta = X_c^2 B X F(X) dX \tag{15}$$

Thus,

$$g(t,\theta) = \frac{\int_X^{\infty} X\ F(X)dX}{\int_0^{\infty} X\ F(X)dX} = g(t,X) \tag{16}$$

A polynomial least-square fit to the F(X) data of Marion and Zimmerman was made in order to perform the above integrals in Eq. (16). The Marion and Zimmerman tables include values of F(X) for only relatively small values of X, whereas fairly large values often are required for shielding purposes. At large X values (and consequently, large θ*),Rutherford single scattering dominates, which may be described by $K_1/\sin^4(\theta/2) = K/X^4$ where K is a constant determined by normalizing to the last data point given by Marion and Zimmerman. A similar normalization to the Fermi-Eyges theory could have been made, but has not been included in this paper since Eq. (1), and hence Eq. (5), are of the form generally used to estimate beam scattering around accelerators.

Figure 2 gives g(t, X) versus X for various values of B. Table I gives the values of B and $X_c\sqrt{B}$ to use for various target materials and thicknesses, and

*Note: θ is still small enough, however, to make the approximation $\sin\theta \simeq \theta$.

for an electron energy of 1 GeV. The parameter B depends only on the target material and thickness through Eqs. (11) and (12), whereas $X_c\sqrt{B}$ also depends on energy through Eq. (14). Thus, the value of $X_c\sqrt{B}$ can be scaled by dividing by the electron energy in GeV.

III. DISCUSSION

Table I and Fig. 2 are sufficient for determining the fraction of electrons that scatter out of a cone with a given space angle, θ, for many commonly used target materials. Given a target material and thickness in radiation lengths, values for B and $X_c\sqrt{B}$ are found in Table I. The B value determines which B curve to use in Fig. 2. The abscissa, X, may be converted to θ, (in mradians by Eq. (13).

If in a particular shielding situation, the space angle, θ, as defined by a collimator, entrance flange, etc., is critical, a family of curves may be constructed for different target thicknesses showing the change in $g(t,\theta)$ with changes in incident beam energy. Figure 3 shows such a set of curves for $\theta = 4.17$ mradians with four different thicknesses of copper.

For comparison, both the Fermi-Eyges derived expression, (Eq. 5), and the fraction that escapes as determined by Molière theory, (Eq. 16), using Table I and Fig. 2, are plotted in Fig. 1 for a given target thickness and energy. It is apparent that the Fermi-Eyges expression overestimates the scattering at small angles (by as much as a factor of two) while seriously underestimating scattering at larger angles. The relative shapes of the Molière and Fermi-Eyges curves are independent of energy. That is, the point of intersection of the two curves will have the same value of $g(t,\theta)$ for a given target thickness irrespective of energy (as energy changes, the abscissa, θ, changes but the shapes remain the same). Also, this crossover value, where $g(t,\theta)$ is the same for both curves, varies only a small amount with changes in target thickness (see Fig. 4). Thus, for example, if a $g(t,\theta)$ value of 4×10^{-2} or greater is acceptable from a shielding standpoint, one could use the Fermi-Eyges expression, Eq. (5), to determine θ out to $g(t,\theta) = 4 \times 10^{-2}$, and be conservative. If a value of $g(t,\theta) = 4 \times 10^{-2}$ is too large in terms of prospective radiation hazards, then the more exact scattering theory (Fig. 2 and Table I) must be used.

The above arguments all assume that the incident beam has no size or angular distribution (i.e., may be described by a delta function). In practice, this often is not the case; not only may the beam have dimension, but it also may be diverging. We recently measured the differential scattering from a 0.1 radiation length copper target and for a 10 GeV incident positron beam (differences in electron scattering and positron scattering are small[7], and should not be noticeable in the measurements). Figure 5 shows the differential distribution, F(X), as measured, and as would be calculated (normalized to unity at X = 0). As can be seen, there is a large disparity between curves. Glass slides inserted first at the target position and later downstream showed a considerable beam divergence with no target inserted. Because of the limited range of the glass slides, it was impossible to determine if the divergence were described by a Gaussian, or if it were already multiple scattered by some obstacle upstream.

Finite beam conditions must be folded into any determination of F(X), which also changes the shape of g(t, X). Any spread in beam size, or any divergence, should act in the direction of increasing F(X). If the divergence is Gaussian, as might be the case in the bunching of particles during acceleration, the effect will be seen mainly in the region of multiple or plural scattering (where each B curve may be thought of as having three distinct parts--a region of multiple scattering described adequately by a Gaussian, a long tail caused by single scattering and a region joining the two that is called plural scattering). There will be only a small effect at large values of X where single scattering dominates. However, if the beam has already undergone some scattering prior to multiple scattering in the target, the effect will be felt both in the regions of plural and single scattering, i.e., at large values of X.

Consider a beam with an angular distribution, $I(X_\phi)$, incident upon a target. It can be shown that[8]

$$F'(X) = 2\int_{X_\phi=0}^{\infty} \int_{\rho=0}^{\pi} X_\phi I(X_\phi)\, F(X_\alpha)\, dX_\phi d\rho \tag{17}$$

where $F'(X)$ = multiple scattering distribution with incident beam distribution included

$F(X_\alpha)$ = multiple scattering distribution according to Eq. (6)

$I(X_\phi)$ = angular distribution of the incident beam

and where the azimuthal angle of integration, ρ , and the reduced angles X, X_α and X_ϕ are related by[8]

$$X_\alpha^2 = X^2 + X_\phi^2 - 2XX_\phi \cos \rho \tag{18}$$

For the case of an input beam distribution in the form of a delta function, this should reduce to $F(X_\alpha)$. This can be shown as follows.

Let the incident beam distribution be a delta function of the form

$$I(X_\phi)\, X_\phi\, dX_\phi\, d\rho = \frac{1}{2\pi}\, \delta(X_\phi)\, dX_\phi d\rho \tag{19}$$

so that

$$\int_{X_\phi=0}^{\infty} \int_{\rho=0}^{2\pi} I(X_\phi)\, X_\phi\, dX_\phi d\rho = 1 \tag{20}$$

Substitution into Eq. (17) gives

$$F'(X) = F(X_{\alpha}). \tag{21}$$

Figure 6 compares Eq. (17) with the experimental results shown in Fig. 5, where the incident angular distribution, $I(X_{\phi})$, is represented by a delta function, a Gaussian, and a multiple scattered shape. The values for the latter two were determined from the glass plate exposures. As can be seen, predicting a scattering source upstream comes closer to explaining the measurements at relatively small values of X than does the use of a Gaussian input. For values of X greater than 5, where the effect of the single scattering normalization dominates, neither input satisfactorily predicts the measurements. This does not necessarily imply that the single scattering addition is inadequate, since the glass plates did not provide any information as to the shape of the input distribution at large values of X. The positron beams at SLAC, as compared to the electron beams, have an inherently large phase space due to the method of production, which results in a relatively large angular distribution. The uncertainty in input beam shape may explain the above disagreement.

Even though this particular experiment using a positron beam did not agree well with calculation, we have used the curves of Fig. 2 and Table I many times to predict radiation levels from high energy electron beams, and have found good agreement with measurements.

REFERENCES

1. L. Eyges, "Multiple Scattering with Energy Loss," Phys. Rev. 74, 1534 (1948).
2. B. Rossi, High-Energy Particles, Prentice-Hall, Englewood Cliffs, New Jersey, 1952; B. Rossi and K. Greisen, "Cosmic-Ray Theory," Rev. Mod. Phys. 13, 240 (1941).
3. W. H. Barkas, Nuclear Research Emulsions, Vol. I, Techniques and Theory, Academic Press, New York and London (1963).
4. G. Molière, Z. Naturf, 2a, 133 (1947); Z. Naturf. 3a, 78 (1948).
5. B. P. Nigam, M. K. Sundaresan, and T. Y. Wu, "Theory of Multiple Scattering: Second Born Approximation and Corrections to Molière's Work," Phys. Rev. 115, 491 (1959).
6. J. B. Marion and B. A. Zimmerman, "Multiple Scattering of Charged Particles," Nucl. Instr. and Methods 51, 93 (1967).
7. B. P. Nigam and V. S. Mathur, "Difference in Multiple Scattering of Electrons and Positrons," Phys. Rev. 121, 1577 (1961).
8. W. R. Nelson, "The Shielding of Muons Around High Energy Electron Accelerators: Theory and Measurement," Report No. SLAC-PUB-481, Stanford Linear Accelerator Center, Stanford University, Stanford, California (1968); to be published in Nucl. Instr. and Methods.

TABLE I

VALUES OF B AND $X_c\sqrt{B}$ FOR DIFFERENT MATERIALS.

(VALUES OF $X_c\sqrt{B}$ ARE IN MRADIANS FOR E_0 = 1 GeV; t IN RADIATION LENGTHS)

B	Aluminum		Beryllium		Copper		Hydrogen		Iron	
	t	$X_c\sqrt{B}$	t	$X_c\sqrt{B}$	t	$X_c\sqrt{B}$	t	$X_c\sqrt{B}$	t	$X_c\sqrt{B}$
8	.0035	.8489	.0018	.5731	.0055	1.1092	.0008	.3610	.005	1.0695
	.004	.9072	.002	.6064	.006	1.1578	.002	.5593	.006	1.1471
	.005	1.0143	.003	.7427	.007	1.2506	--	--	.007	1.2390
	.006	1.1111	.004	.8576	.008	1.3369	--	--	.008	1.3246
	.007	1.2001	--	--	.009	1.4180	--	--	.009	1.4049
	.008	1.2829	--	--	.01	1.4947	--	--	.01	1.4809
9	.0084	1.3944	.0043	.9414	.013	1.8220	.002	.5593	.0125	1.7569
	.009	1.4433	.005	1.0169	.02	2.2421	.003	.7265	.02	2.2214
	.01	1.5214	.006	1.1140	.03	2.7460	.004	.8389	.03	2.7206
	.02	2.1515	.007	1.2033	--	--	--	--	--	--
	--	--	.008	1.2863	--	--	--	--	--	--
	--	--	.009	1.3644	--	--	--	--	--	--
	--	--	.01	1.4382	--	--	--	--	--	--
10	.0204	2.2923	.0104	1.5476	.032	2.9952	.0049	.9749	.0304	2.8881
	.03	2.7776	.02	2.1439	.04	3.3423	.005	.9887	.04	3.3114
	.04	3.2073	--	--	.05	3.7368	.006	1.0831	.05	3.7023
	.05	3.5859	--	--	.06	4.0935	.007	1.1698	.06	4.0557
	--	--	--	--	.07	4.4215	.008	1.2506	.07	4.3806
	--	--	--	--	--	--	.009	1.3265	--	--
	--	--	--	--	--	--	.01	1.3982	--	--
11	.0503	3.7704	.0256	2.5454	.079	4.9265	.012	1.6035	.075	4.7504
	.06	4.1199	.03	2.7539	.08	4.9575	.02	2.0739	.08	4.9117
	.07	4.4500	.04	3.1799	.09	5.2582	--	--	.09	5.2096
	.08	4.7572	.05	3.5552	0.1	5.5426	--	--	0.1	5.4914
	.09	5.0458	.06	3.8946	--	--	--	--	--	--
	.1	5.3187	--	--	--	--	--	--	--	--

FIGURE CAPTIONS

1. The fraction of electrons, $g(t,\theta)$, that escapes a cone with a space angle θ, for a 0.07 radiation length copper target and with an incident electron energy, $E_o = 1$ GeV.
   a. Dashed line from Eq. (5).
   b. Solid line from Eq. (16) using Fig. 2 and Table I.
2. The fraction of electrons, $g(t, X)$, that escapes a cone with a space angle $X = \theta/X_c \sqrt{B}$, versus X, for values of B from 7 through 12.
3. The fraction of electrons, $g(t,\theta)$, that escapes a cone with a space angle, $\theta = 4.17$ mradians, versus the electron energy, E_o, for several copper target thicknesses.
4. The value of $g(t, \theta)$ where Eq. (5) equals Eq. (16) versus the target thickness (copper) in radiation lengths.
5. Comparison of the measured and theoretical differential distribution function, $F(X)$, for a 10 GeV positron beam incident upon a 0.1 radiation length copper target. The solid line is the theoretical calculation of Marion and Zimmerman; the dashed line was drawn through the data by eye.
6. The effect of a finite input beam on the differential distribution function, $F(X)$, where $F'(X)$ is given by Eq. (17). Curve A - Delta function input. Curve B - Gaussian input. Curve C - Multiple scattered input. X - Data points for a 10 GeV positron beam incident upon a 0.1 radiation length copper target.

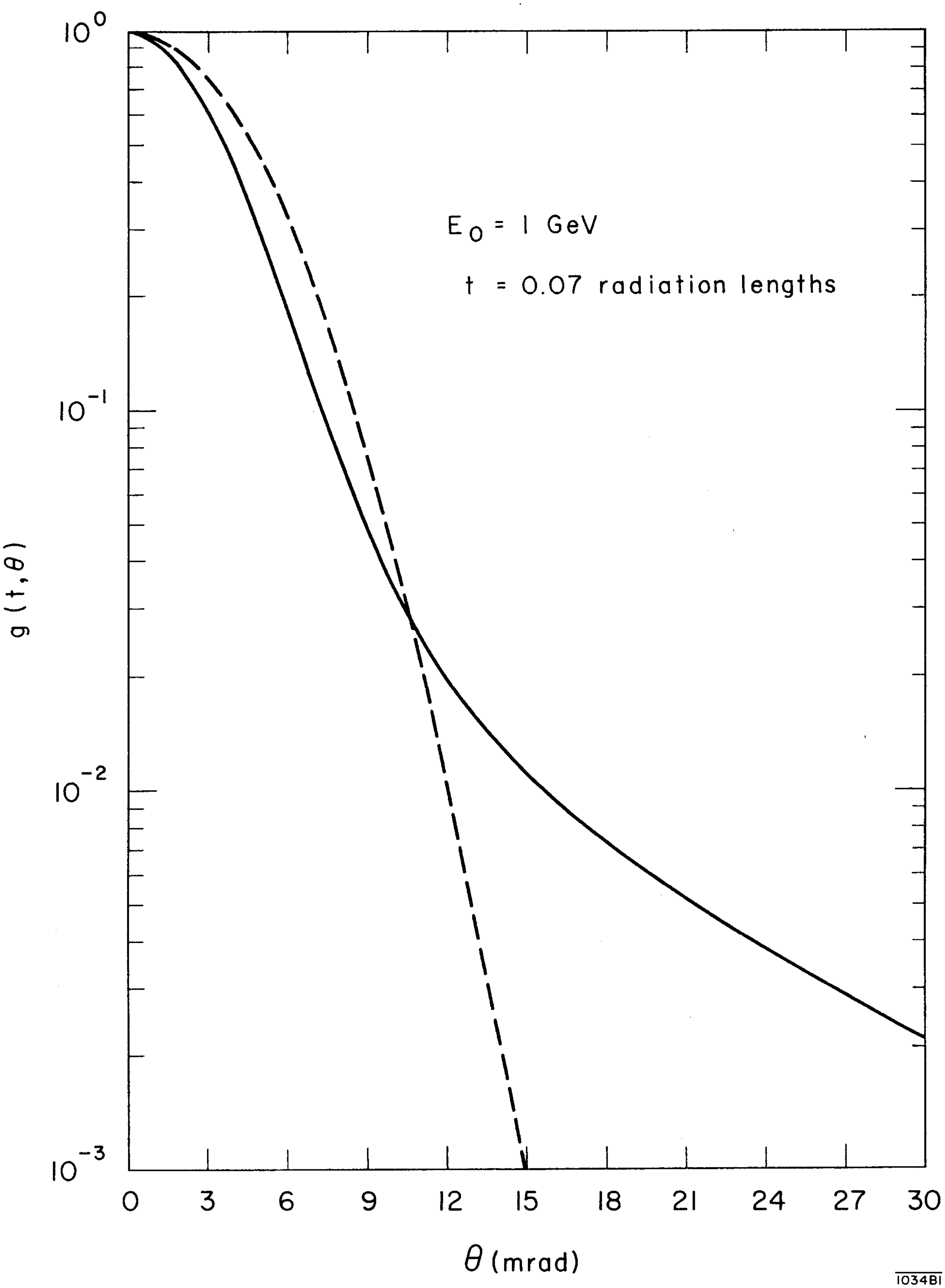
10^0
10^{-1}
10^{-2}
10^{-3}
E_0 = 1 GeV
t = 0.07 radiation lengths
g (t, θ)
0
3
6
9
12
15
18
21
24
27
30
θ (mrad)
1034B1

Fig. 1

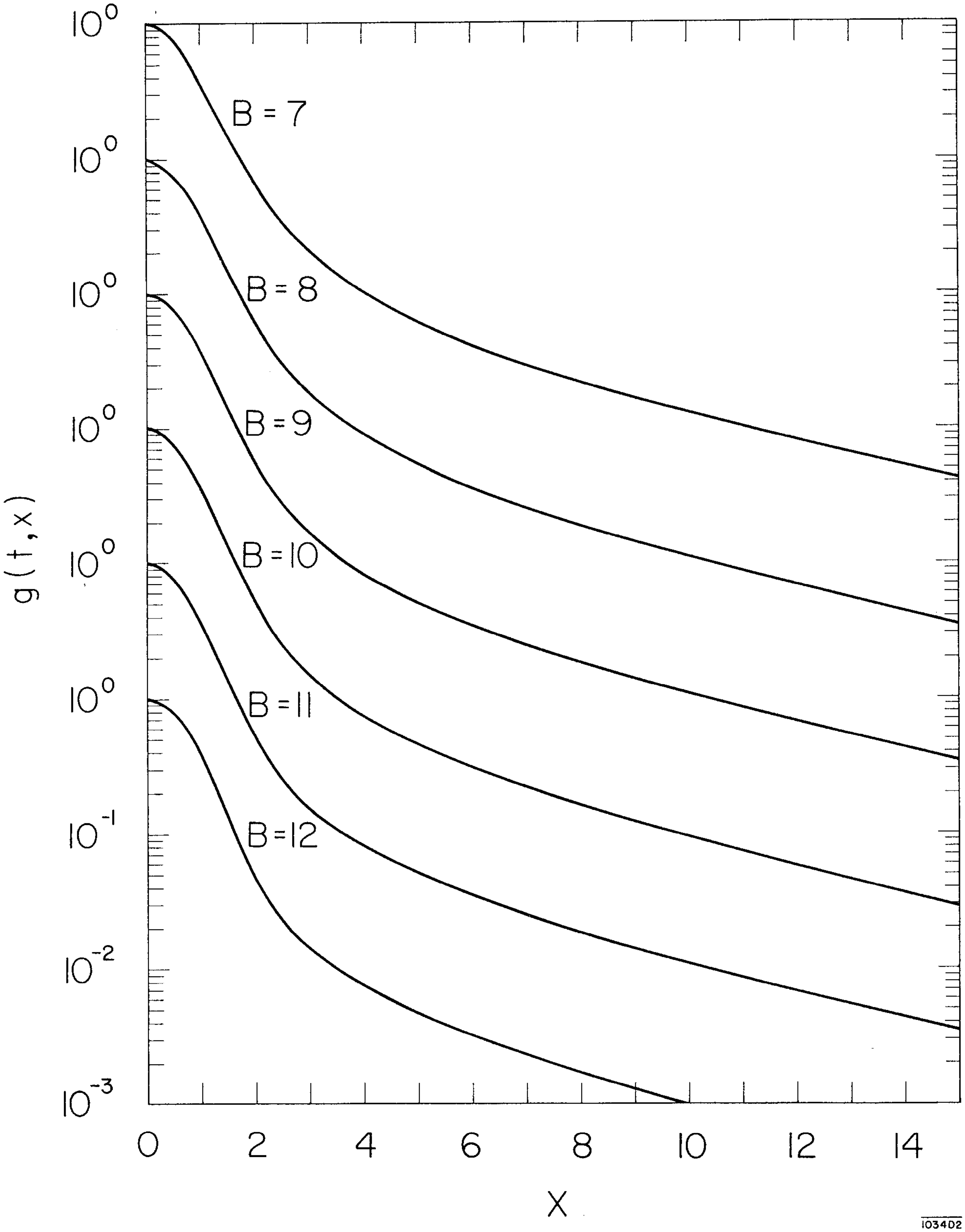
B = 7
B = 8
B = 9
B = 10
B = 11
B = 12
10^0
10^0
10^0
10^0
10^0
10^0
10^{-1}
10^{-2}
10^{-3}
g(t, x)
0
2
4
6
8
10
12
14
X
103402

Fig. 2

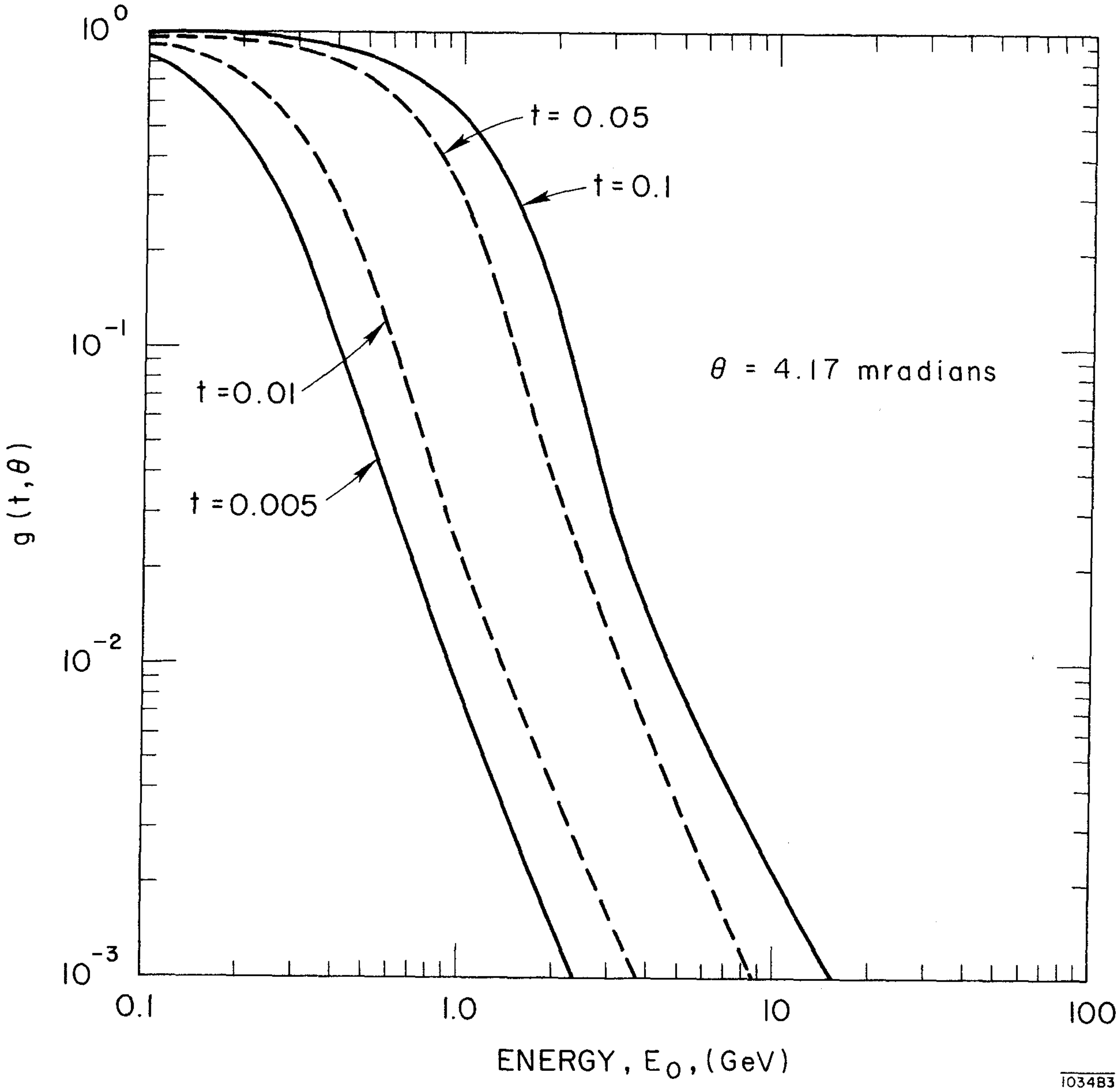

t = 0.05
t = 0.1
t = 0.01
t = 0.005
θ = 4.17 mradians
g (t, θ)
10^0
10^{-1}
10^{-2}
10^{-3}
0.1
1.0
10
100
ENERGY, E_0, (GeV)
1034B3

Fig. 3

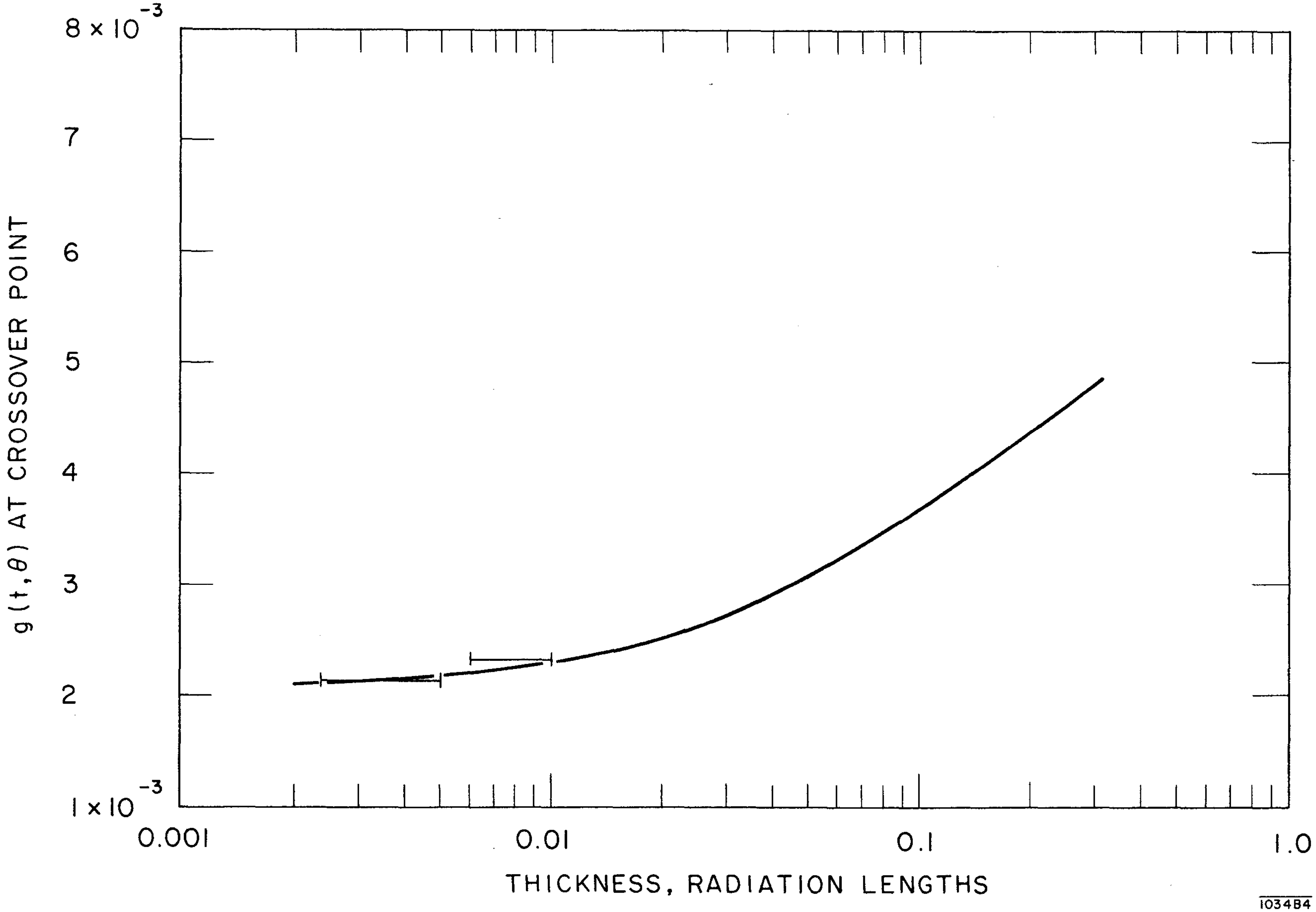

8 × 10^-3
7
6
5
4
3
2
1 × 10^-3
g (t, θ) AT CROSSOVER POINT
0.001
0.01
0.1
1.0
THICKNESS, RADIATION LENGTHS
1034B4

Fig. 4

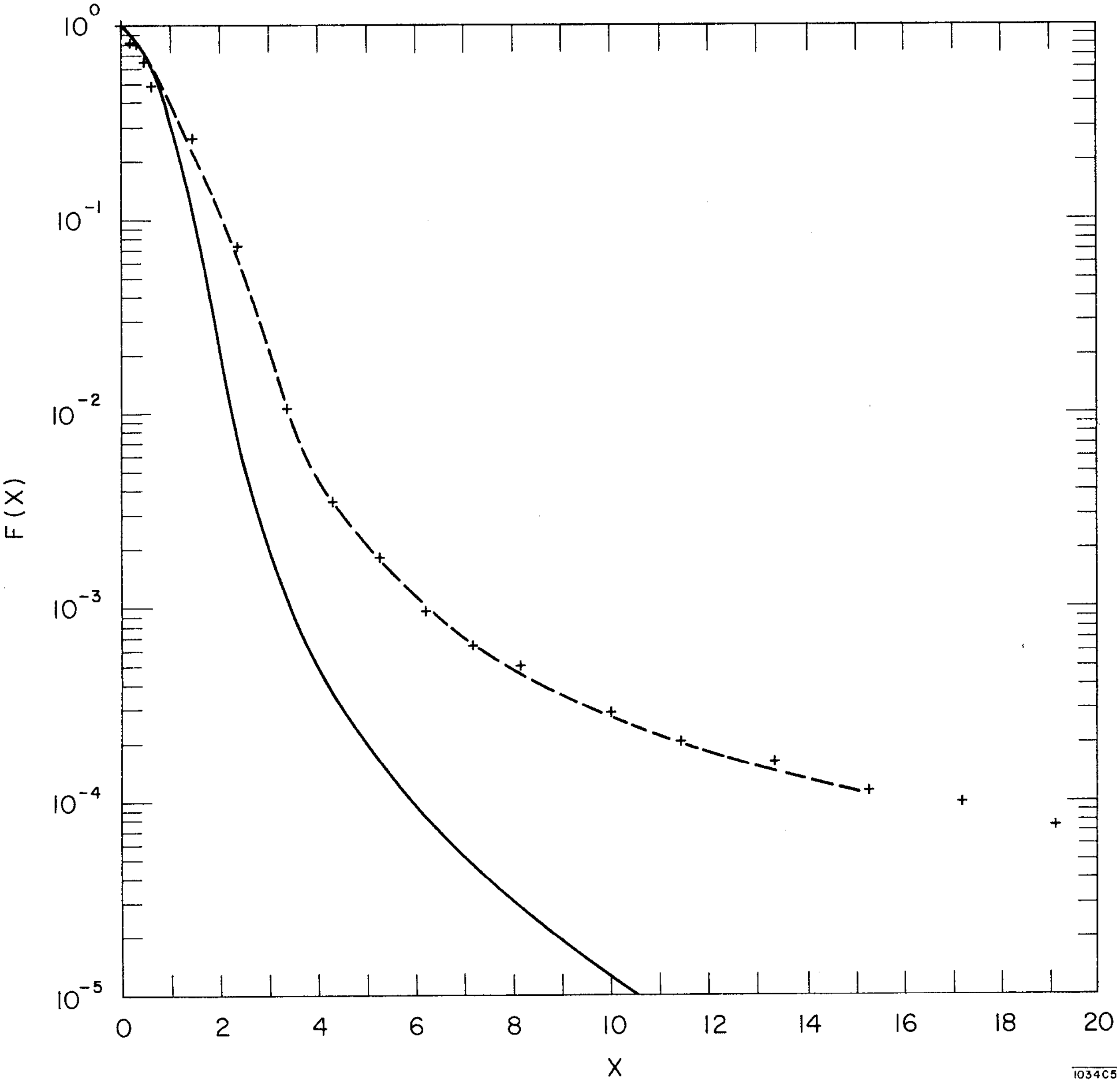

Fig. 5

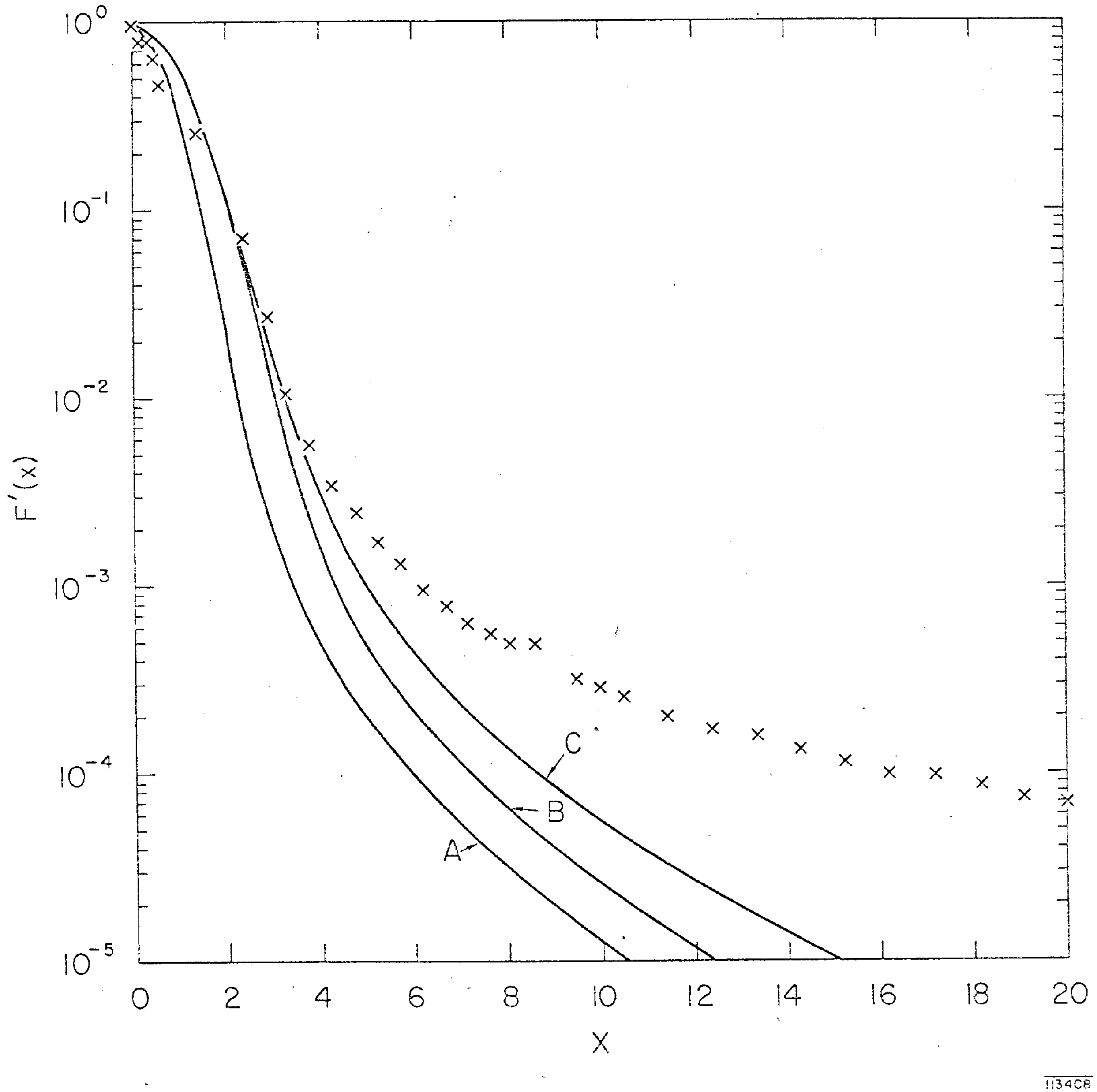

Fig. 6